

DIRC DREAMS REDUX: RESEARCH DIRECTIONS FOR THE NEXT GENERATION OF INTERNALLY REFLECTED IMAGING COUNTERS^{*}

Blair N. Ratcliff

Stanford Linear Accelerator Center, Stanford University, Stanford, California 94309, USA

Abstract

Some general conceptual design features of total internally reflecting, imaging Cherenkov counters (DIRCs) are described. Limits of the DIRC approach to particle identification and a few features of alternative DIRC designs are briefly explored.

1. Introduction and Scope

The DIRC, for **D**etection of **I**nternally **R**eflected **C**herenkov (Light), is a subtype of **R**ing **I**maging **C**herenkov counter (RICH). It “inverts” the usual principle for use of light from the radiator of a RICH by collecting and imaging the total internally reflected light, rather than the transmitted light. In so doing, a DIRC utilizes the optical material of the radiator in two ways, simultaneously; first, as a Cherenkov radiator, and second, as a light pipe for the Cherenkov light trapped in the radiator by total internal reflection. The high reflection coefficients inherent in the total internal reflection process, and the fact that the magnitudes of angles are conserved during reflection from a flat surface allow the photons of the ring image to be transported to a detector outside the path of the radiating particle, where they may be imaged [1-2].

A number of DIRC prototypes have been constructed and tested over the past few years [3-8]. The first large-scale DIRC detector designed for physics is now running in the BABAR detector at PEP-II [9]. This detector uses a radiator of 144-long fused silica bars ($1.7 \times 3.5 \times 490 \text{ cm}^3$) arrayed as a

^{*}Work supported by Department of Energy contract DE-AC03-76SF00515.
Submitted to ICFA Instrumentation Bulletin, April 2001.

12-sided polygon around the PEP-II interaction region. These bars are coupled to an $\sim 11,000$ photomultiplier tube (PMT) array through a 120 cm long standoff region filled with purified water. Though the performance of this device is excellent and well-matched to the particular requirements of an asymmetric B-factory like PEP-II, some design features, particularly the very long bars and the large water-coupled detection system, are less than ideal (at least aesthetically). The large water tank increases the susceptibility of the device to soft gamma background from the machine, and the overall design is rather inflexible geometrically. The basic features of this design were driven by “practical” compromises between detector performance on the one hand, and availability, timeliness, risk, and cost of components on the other. In particular, although reflectively focused schemes with better timing resolution were considered [10], the lack of any well-validated, cost-effective alternative to “standard” PMTs as the photon detector was a determining factor in reaching this design. With “standard” PMTs, one is naturally led to a large photon detection plane, water coupling, and the long bars to bring the light to the PMTs in a region that can be shielded from the magnetic field. During the intervening years, photon detectors have evolved, and it is interesting to look at how this evolution might affect some of the practical possibilities for DIRC, and what continued developments might portend for the future. This paper will attempt to clarify some of the issues discussed previously (see, e.g., the talk at RICH98 [11]), and in particular, will include a more complete, pedagogical discussion of the role of time resolution in DIRC counters.

2. Basic Cherenkov Equations

As is well-known, Cherenkov radiation is emitted at polar angle (θ_c), uniformly in azimuthal angle (ϕ_c), with respect to the particle path

$$\cos \theta_c = \frac{1}{\beta n(\lambda)}, \quad (1)$$

where $\beta = v_p/c$. v_p is the particle velocity, c is the speed of light, and $n(\lambda)$ is the index of refraction of the material. Since the index of refraction is a function of the photon wavelength, in normal optical materials there is an “intrinsic” Cherenkov angle resolution limit that depends on the detected photon bandwidth.

The number of photoelectrons observed (N_{pe}) is given by the Frank-Tamm equation,

$$N_{pe} = 370L \int \varepsilon \sin^2 \theta_c dE, \quad (2)$$

where L is the length of the particle through the radiator in cm, $\varepsilon(E)$ is the overall collection efficiency for the Cherenkov photons multiplied by the detection efficiency for observing these photons as photoelectrons, and E is the photon energy in eV.

Although it was first discussed in a classical paper by Tamm in 1939 [12], it seems to be little appreciated that the conical Cherenkov radiation shell is not perpendicular to the Cherenkov propagation angle in a dispersive medium. The half-angle of the cone opening (η) is given by,

$$\cot \eta = [(n(\omega_0)\beta)^2 - 1]^{1/2} + \omega_0 n(\omega_0)\beta^2 (dn/d\omega)_0 [(n\beta)^2 - 1]^{-1/2}, \quad (3)$$

where the index of refraction $n(\omega)$ is written as a function of the angular frequency of the Cherenkov light (ω), and the frequency range is centered at ω_0 . As Motz and Schiff pointed out in 1953 [13], the presence of the second term means that the cone angle (η) is the complement of the Cherenkov angle (θ_c) only for a nondispersive medium where $dn/d\omega = 0$. In dispersive optical material, the Cherenkov cone is no longer perpendicular to the direction of photon propagation, but can instead be thought of as side-slipping as it moves along with the charge.

3. The DIRC Principle

The geometry of a single radiator of a reference conceptual DIRC is shown schematically in Fig. 1. Each radiator is a long, thin bar with a rectangular cross section of transverse dimensions (t_x, t_y). A track with velocity β passing through the radiator with refractive index (n_1) emits Cherenkov radiation in a cone around the particle trajectory. The source length of the light emitting region is the particle trajectory length in the radiating material. The angles, positions, momentum (and timing) of the track are normally provided by other detectors, primarily by a tracking device located in front of the radiator, and perhaps by the crossing time of the beams in the machine. If the index of refraction of the radiating material (n_1) substantially exceeds $\sqrt{2}$, and the index of the

surrounding material (n_3) is approximately one, then for a particle close to $\beta = 1$, some portion of the light will always be transported down the bar to the end. Since the radiator cross section is rectangular, the magnitudes of the angles are maintained by reflections at the surfaces of the bar. Thus, in a perfect bar, the portion of the Cherenkov cone that lies inside the total internal reflection angle is transported undistorted down the bar to the end (except for additional up-down/left-right ambiguities).

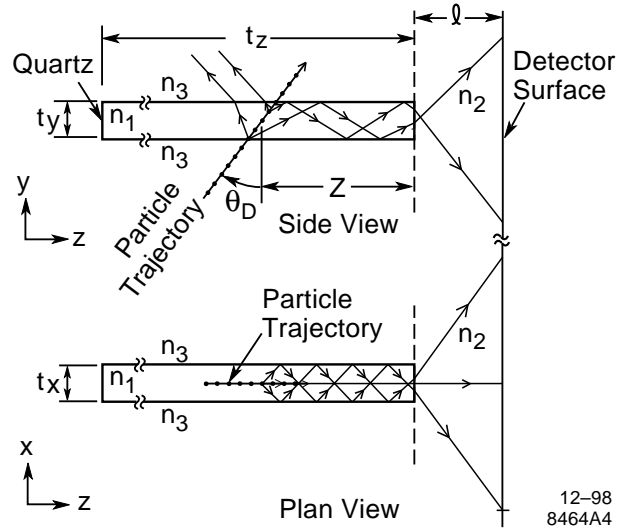


Figure 1. Schematic of a radiator bar illustrating the principle of the DIRC. The particle trajectory is shown as a line connected by dots; representative trajectories of Cherenkov photons are shown as lines with arrows.

The Cherenkov photons are imaged onto a detector located outside the particle path. Although there are only two Cherenkov emission angles (θ_c , ϕ_c) of interest for particle identification, the DIRC is intrinsically a three-dimensional imaging device.[†] The directly measurable quantities are usually the space-position of each “hit” in a detector “pixel” (e.g., a PMT), and its associated time. The space-position provides a direct measurement of the two normal angles with respect to the end of the bar (α_x , α_y), assumed here to be corrected for refraction so that they are the angles inside the bar material. The third angle (α_z) can be calculated from the constraint. However, because of the long

[†] A number of DIRC devices have been proposed that use less than three dimensions. For example, a 1-D device (called the CCT) that couples DIRC bars with a non-imaging detection system that times the first photoelectron(s) seen at the bar end was proposed by Honscheid *et al.* [17]. A prototype has been constructed and tested by Kichimi *et al.* [7]. Akatsu *et al.* [8] have proposed and tested a 2-D readout DIRC (one timing dimension and one space dimension) called the TOP counter.

optical delay line, the photon propagation time down the bar [t_p , see Eq. (6) below] is also directly related to the direction cosine of the photon angle along the bar z axis (α_z). This over constraint is quite powerful in rejecting backgrounds and ambiguous solutions. It is usually only necessary to instrument one end of the bar, and reflect photons heading the “wrong” way back to the detector. The propagation time shift between the forward and backward going photons usually makes them easy to separate.

For pedagogical purposes, it may be useful to write down specifically how the measured quantities are related to Cherenkov angles. Consider a frame (\underline{k}) where the particle moves along the (z) axis. The direction cosines of the Cherenkov photon emission in this frame (\underline{k}_x , \underline{k}_y , and \underline{k}_z), are related to the Cherenkov angular definition [see Eq. (1)] by,

$$\begin{aligned}\underline{k}_x &= \cos \varphi_c \sin \theta_c, \\ \underline{k}_y &= \sin \varphi_c \sin \theta_c, \\ \underline{k}_z &= \cos \theta_c.\end{aligned}\tag{4}$$

Now consider the right-handed coordinate system attached to the bar frame as indicated in Fig. 1. In this frame, we call the track polar and azimuthal angles (θ_t , φ_t). We then align the \underline{k} frame x-axis such that the direction cosines of the photon emission in the bar frame can be written as

$$\begin{aligned}k_x &= -\underline{k}_x \cos \theta_t \cos \varphi_t + \underline{k}_y \sin \varphi_t + \underline{k}_z \sin \theta_t \cos \varphi_t, \\ k_y &= -\underline{k}_x \cos \theta_t \sin \varphi_t - \underline{k}_y \cos \varphi_t + \underline{k}_z \sin \theta_t \sin \varphi_t, \\ k_z &= \underline{k}_x \sin \theta_t + \underline{k}_z \cos \theta_t.\end{aligned}\tag{5}$$

The photon propagates a length (L_p), in a time (t_p), down a bar length of (L) as is given by

$$t_p = \frac{L_p n_g}{c} = \frac{L n_g}{c k_z},\tag{6}$$

where the photon group velocity ($v_{\text{group}} = c/n_g$) must be used rather than the photon phase velocity ($v_{\text{phase}} = c/n$) since, in a dispersive medium, energy propagates at the photon group velocity. The connection between Eqs. (3) and (6) should be noted. The relationship between group and phase

velocities, as a function of photon wavelength (λ), is usually derived in a simple one-dimensional picture [14], and leads to the following relationship between the group and phase refractive indices:

$$n_g(\lambda) = n(\lambda) - \lambda \frac{dn(\lambda)}{d\lambda}. \quad (7)$$

For fused silica, $n_g(\lambda)$ is typically several percent larger than $n(\lambda)$ for photons in the energy range detectable by a bi-alkali photo-cathode. As a particular example, the weighted averaged value

$$\left\langle \frac{n(\lambda)}{n_g(\lambda)} \right\rangle \sim 0.97 \text{ for photons from a Cherenkov spectrum impinging on a bi-alkali photocathode}$$

after passing through a borosilicate window. The dispersion of n_g is also substantially greater.

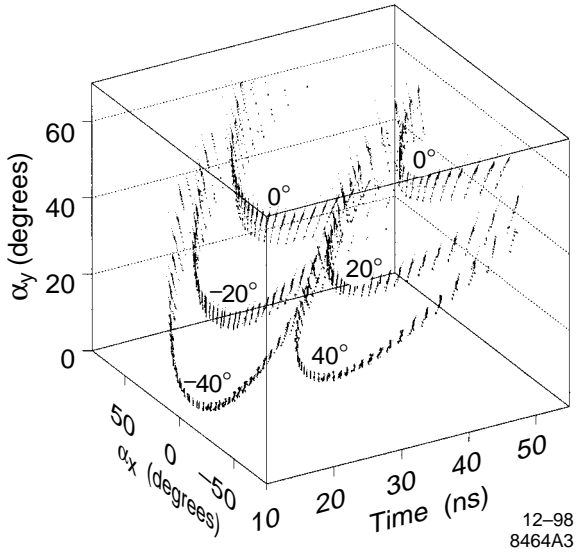


Figure 2. Three-dimensional images (α_x, α_y, t_p) of Cherenkov photons produced by tracks at dip angles of 0° , $\pm 20^\circ$, and $\pm 40^\circ$ in a 5-m long DIRC. Measurements are made at only one bar end, with photons reflected at the other end. The tracks enter normal to the DIRC bar, so there are no left-right ambiguities.

A simplified view of the measurement space for tracks entering a DIRC bar at three different dip angles (in a DIRC bar similar to that of the BaBar DIRC) is shown in Fig. 2.

4. DIRC Design Choices

The following sections briefly review some of the choices one must make in designing a DIRC, with an eye to providing a framework for considering some possible design directions. The BABAR DIRC design provides a basic reference set of choices. Of course, there are other options and

combinations possible, but only a few can be discussed in any detail. This discussion will focus on choices that appear to be most technically feasible.

4.1 Cherenkov Light Production

Fused silica is the logical material for the radiator, and has been used for all DIRCs built to date. It is very transparent, has a rather uniform index of refraction, modest dispersion in the visible, can be ground with sharp corners, and takes a good polish. Synthetic fused silica is also very hard against ionizing radiation. Its most serious liabilities are that it is expensive to procure and process; it has a rather short radiation length ($X_0 = 12.3$ cm); and it can also have small periodic fluctuations in index which can lead to diffractive effects at some transmission angles [18]. One potentially promising area to explore would be the use of plastics, particularly in an end-cap or fixed-target environment, where transmission distances can be reasonably short. This might allow a molded radiator to be made at a large savings in cost. In particular, acrylic is known to have transmission coefficients in the 10 m range for photon wavelengths above 400 nm [1,2,7]. It also has fair reflection coefficients provided that the cast surfaces can be used [7,15]. It is inexpensive to procure and has a long radiation length ($X_0 = 34.4$ cm), so that one can partially compensate for light loss during transmission by making the radiator thicker. However, it remains to be demonstrated whether one can obtain the index uniformity, edge sharpness, and surface and figure quality from cast surfaces to make such a detector feasible. In any case, plastic is radiation soft, which will further limit potential applications.

4.2 Cherenkov Light Transport

The principle design issue is whether the light guide width-to-thickness ratio is such that photons reflect many times in one dimension only, or in two dimensions. This issue has been discussed previously, where the different choices were called “plates” (reflection many times only in one dimension) and “pipes” (reflection many times in two dimensions) [1,2]. In a DIRC of the BaBar type, which uses “pipes,” both transverse dimensions of the radiator bar are small and the length is long, so that the precise photon path and number of bounces are lost, or at least not utilized. The image is then essentially length independent. However, since many bounces occur from all the sides and faces in this approach, a premium is placed on the sharpness of the side/face edges, since photons will get lost in the corners if the edges are not sharp. If there are many bounces from the

sides, one also depends on the orthogonality of the angles between sides and faces. On the other hand, if one dimension of the radiator is sufficiently wide, it is possible to track the photon path from production to detection in the wide dimension. An example of such a situation is an end-cap device [5]. A plate design allows the entire propagation length to be used as the standoff distance. This may improve the resolution, and the properties of the plate sides and side/face edges become less critical. However, one must then keep track of all bounces in this side-to-side plane, and the number of ambiguities will be dependent on the length-to-width ratio. Time information can be useful to help resolve these ambiguities.

4.3 Cherenkov Imaging (Focusing)

As described earlier, the direction of a photon in space is measured and then translated into a measurement of the Cherenkov angles using knowledge of the track direction. In the literature, there are shades of meaning that have been attached to the word “focusing” in the DIRC imaging process. On the one hand, it has been used to refer specifically to an optical system in which light is focused onto the detector by a reflecting lens (see, e.g., Refs. 1,2,5,8,16). On the other hand, it can be argued that all DIRC (indeed all RICH) counters must focus, in that there are no detectors in this energy regime which measure photon angles directly, and so angles must always be derived by a focusing system of some kind. In this view, the differences among imaging systems are more a question of performance properties and complexity of the focusing system employed, rather than differences in basic principles. In any event, the presence of the DIRC light guide does lead to somewhat different considerations for DIRC images than is generally the case for a RICH. In particular, two of the methods described below, the “pinhole” and “time” methods are peculiar to the DIRC.

In Fig. 3, a number of different kinds of DIRC imaging systems are demonstrated schematically, along with a simple “ball park” estimate for the resolution properties of the particular systems. Imaging can be thought of as occurring separately in each of the three dimensions (x, y , and t_p) and different schemes for each dimension can be used in the same counter. Since there are only two Cherenkov angles to be determined, in principle, measurement of only two of these dimensions are

required in any given counter. However, measurement of the third dimension is extremely useful to reject backgrounds and ambiguities, and perhaps provide Cherenkov angle measurement constraints.

The analog of the classic “proximity” focusing scheme, typically used for liquid/solid radiator RICH counters, is shown in Fig. 3(a) for the DIRC. In this scheme, the photon's angles are measured by comparing its detected position with respect to its emission point along the track. This requires knowledge of the position of the input track and the path of the photon to the detector. Note that the relevant “standoff” length may be much longer than the path in the detector box (see method (b) below), so that there could be excellent resolution per photon in the “proximity” focused direction. For example, the “standoff” for the BaBar DIRC is about 117 cm, while the bars are nearly 500 cm long. The price paid for this improved resolution is that the bar bounce ambiguities must be resolved. Excellent time resolution can help. However, to use this method in the DIRC would, in most cases, require a “plate” rather than a “pipe” for light transport.

“Proximity” focusing is related to, yet subtly different than, the “pinhole” focusing method used by the BaBar DIRC, as shown in Fig. 3(b). This later imaging scheme is a direct analogue of the pinhole camera, hence the name. In this case, the path of the photon down the bar is ignored, and the resolution is independent of the precise track location in the bar. It does, however, depend directly on the size of the bar exit aperture. The relevant standoff length becomes the distance from the bar end to the detector plane, rather than the distance from the track to the detector plane. This would normally be shorter than for the “proximity” focused scheme of Fig. 3(a).

Figure 3(c) shows one version (a single reflective lens) of “lens” focusing. Other versions of lens focusing could use refractive, gradient, or diffractive lens, but the reflective system has the advantage that it allows the same material in the focusing region as in the bars, thus maximizing the overall efficiency for photon propagation. The advantage of a focusing scheme of this kind, compared to the pinhole scheme, is that the bar size can, in principle, be removed from the resolution. One can also magnify or de-magnify the image to match the pixel size of a particular detector device.

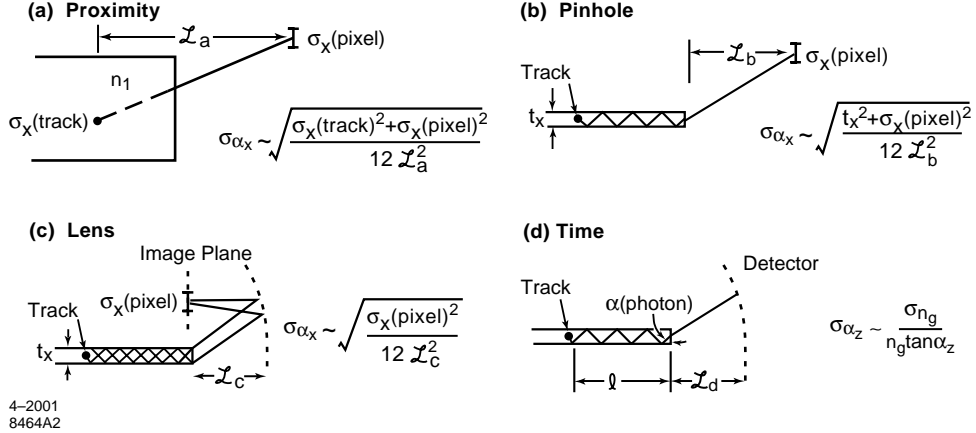


Figure 3. Illustrations of four different DIRC imaging schemes: (a) proximity (b) pinhole (c) lens (d) time. Simple estimates of the imaging and detector part of the resolution obtained on the photon angle in the projection shown are noted for each scheme. These estimates should be treated as pedagogic approximations. For simplicity, all position and detector resolutions are treated as though they are pixelized, and the indices of refraction of the Cherenkov radiator and the imaging region are taken to be the same. The time dimension resolution estimate (d) is given for the dispersion limiting case where the time measurement resolution itself is not the limiting factor. Sec. 4.3 describes the more general case.

Finally, Fig. 3(d) illustrates the principle of the timing dimension. Equation (6) shows that the direction cosine along the z -axis (k_z) is inversely related to the photon propagation time, so that one might naively think that the resolution of such an angle measurement is inversely related to the distance the photon travels down the bar. However, the dispersive component of the group refractive index is large enough to become a dominant component in many real-world cases. In the particular case illustrated in the figure legend, the time resolution per photon is assumed to be so small that the dispersion dominates the resolution of the photon “dip” angle α_z . The fractional

resolution on n_g [$\delta(n_g) = \frac{\sigma(n_g)}{n_g}$] is about 0.015 for bi-alkali tubes, averaged over the Cherenkov

emission spectrum. So in this case, the error $\sigma_{\alpha_z} \sim 0.015/\tan \alpha_z$ varies from a practical minimum of about 9 mrad for large transverse photon propagation angles ($\alpha_z \sim 60^\circ$) in the bar, to an infinite maximum at $\alpha_z = 0^\circ$, where the photon travels along the bar axis. For a typical α_z of $\sim 30^\circ$, the angular error from dispersion alone is ~ 25 mrad.

4.3.1 Timing Resolution Issues

In cases where one is attempting to use timing, either to measure the Cherenkov angle or to sort out ambiguities, the resolution obtainable can be quite complex to calculate. Not only are the angular dependences large, but there are also correlation terms between production, transport, and length dependent terms (see section 5 below). Understanding the details typically requires a full simulation of the specific counter proposed. However, for pedagogical reasons, it is worth considering a few typical cases in a simplified way to illustrate how some of these effects come into play.

4.3.1.1 BaBar DIRC

For the BaBar DIRC, the timing resolution is generally not competitive with the position resolution for the determination of the Cherenkov angles, unless the number of bounces is very large. Therefore, timing is used primarily as a background and ambiguity resolving measurement, although it is also included directly in the overall PID likelihood. The usual practice for BaBar DIRC is to plot the difference between the measured time and the propagation time (t_p), with corrections for the trigger offset and track travel time to the DIRC bars. The measured time resolution on this difference (σ_t) can then be written as

$$\sigma_t = \sqrt{t_p^2 [\delta^2(L_p) + \delta^2(n_g)] + \sigma_{t_0}^2} , \quad (8)$$

where $\delta(L_p) = \frac{\sigma(L_p)}{L_p}$ is the fractional resolution on the propagation length (L_p), $\delta(n_g) = \frac{\sigma(n_g)}{n_g}$ is

the fractional resolution on the group refractive index averaged over the detected Cherenkov photons, and σ_{t_0} is the average resolution of the PMT tubes and electronics system (as calibrated).

In the simple picture that follows, σ_{t_0} has been set to a nominal 1.6 ns. The co-variance terms have been neglected, although they could affect the time dependent piece by as much as 30% or so at some angles.

As noted above, the fractional resolution on n_g is about 0.015 for bi-alkali tubes averaged over the Cherenkov emission spectrum. This term is expected to have a small (negative) length dependence (arising from the wavelength dependent loss of photons down the bar) that has also been neglected. In the limit of where the time resolution is dominated by propagation dispersion (see the discussion of Fig. 3(d) above), the fractional time resolution is simply equal to the fractional resolution on n_g (i.e., ~ 80 ps/m of propagation length).

The fractional resolution on L_p is equal to the fractional resolution in k_z .

$$\delta(L_p) = \delta(k_z) \approx \frac{\sqrt{1 - k_z^2}}{(k_z^2)} k_{xy} \quad (9)$$

However, the analytic calculation, as shown by the last term, in terms of the measured parameters is complex and has been approximated. For simplicity, the effective resolution in the directional cosines as measured in the transverse planes (k_{xy}) has been taken to be a constant and equal in both measurement planes. For Figure 4 below, it is given the value $k_{xy} = 0.0083$ as derived from averaging over the two space dimensions in a pinhole-focusing model for the BaBar DIRC with a constant standoff from the bar end to the detector. Note that this calculation also requires that the projected photon length along the bar be well-known. In practice, this length is determined from the track position and bar geometry.

Figure 4 shows the resolution growth in this model as a function of propagation length for a detector similar to the BaBar DIRC. In this model, the propagation length is mostly a function of the photon propagation dip angle (k_z). Though the resolution increases substantially for long photon propagation lengths (i.e., as k_z gets smaller) and eventually becomes dominated by the term calculated in Eq. (9), the number of photoelectrons with these very long propagation lengths ($\gg \sim 2$ times the minimum in each direction) is actually quite small. At a more typical value for the photon

propagation angle of $\alpha_z = 30^\circ$ ($k_z = 0.867$), the resolution due to the dispersion in n_g is about 5 times larger than the term given by Eq. (9).

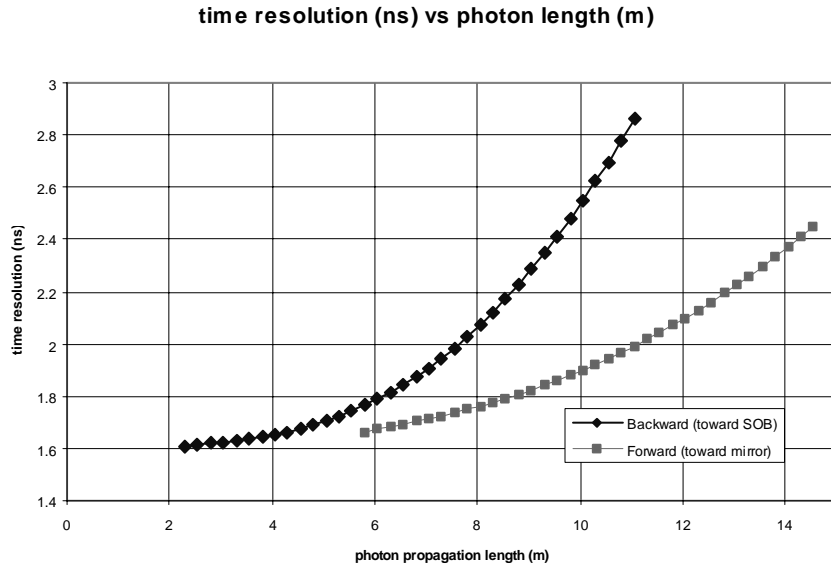


Figure 4. Results of the resolution calculation described in the text for a detector like the BaBar DIRC.

4.3.1.2 Using Time to Measure the Cherenkov Angle

It is worth looking a bit more closely at the way in which the dispersion in the group velocity can effect the measurement of Cherenkov angles when using time imaging. For illustrative purposes, it is useful to consider the special case where the track enters the bar orthogonally in both directions. In the language of equations (4), (5), and (6) we find that

$$k_x = \underline{k}_y = \sin \varphi_c \sin \theta_c,$$

$$k_y = \underline{k}_z = \cos \theta_c,$$

$$k_z = \underline{k}_x = \cos \varphi_c \sin \theta_c.$$

For specificity, consider a device that measures only the propagation time and one (x) angle, e.g.,

$$\tan \alpha_x = \frac{k_x}{k_z},$$

Then,

$$\sin \theta_c = k_z \sqrt{(\tan^2 \alpha_x + 1)}.$$

The resolution on the Cherenkov polar angle per photon is given by,

$$\sigma_{\theta_c}^2 = \tan^2 \theta_c [\delta^2(n_g) + \delta^2(t_p) + \sigma_{\alpha_x}^2 \tan^2 \alpha_x].$$

As a typical numerical example, assume that

$$\tan \theta_c = 1.083, \text{ (i.e., a } \beta = 1 \text{ particle in fused silica)}$$

$$\delta(n_g) = 0.015, \text{ (i.e., a bi-alkali photocathode response curve)}$$

$$\delta(t_p) = \frac{1}{L_p} \left(\frac{100\text{ps}}{5065\text{ps}} \right) = \frac{0.02}{L_p},$$

where L_p is the photon propagation length in meters, and the photodetector resolution is assumed to be 100 ps. We also assume that $\sigma_{\alpha_x} = 0.005$ rad.

Figure 5 shows the results of this calculation of Cherenkov angular resolution per photon as a function of photon propagation length. It should be noted that this particular choice of track angles (that is, zero track dip angle) is the most attractive region for measuring angles with time focusing, and there is relatively little dependence on α_x . However, one can never obtain better than about 16 mrad resolution per photon due to the dispersive component of the group index.

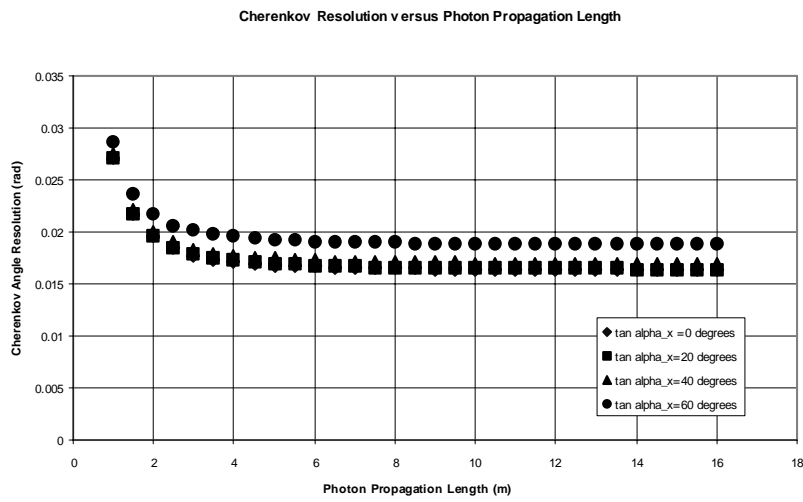


Figure 5. Cherenkov polar angle resolution versus photon propagation length for the special case described in the text. The track is entering the bar normally in both projections.

It is instructive to view the same features plotted as the measured time resolution versus the distance from the track to the detector along the bar for a number of different photon emission angles in the x-plane as shown in Fig. 6.

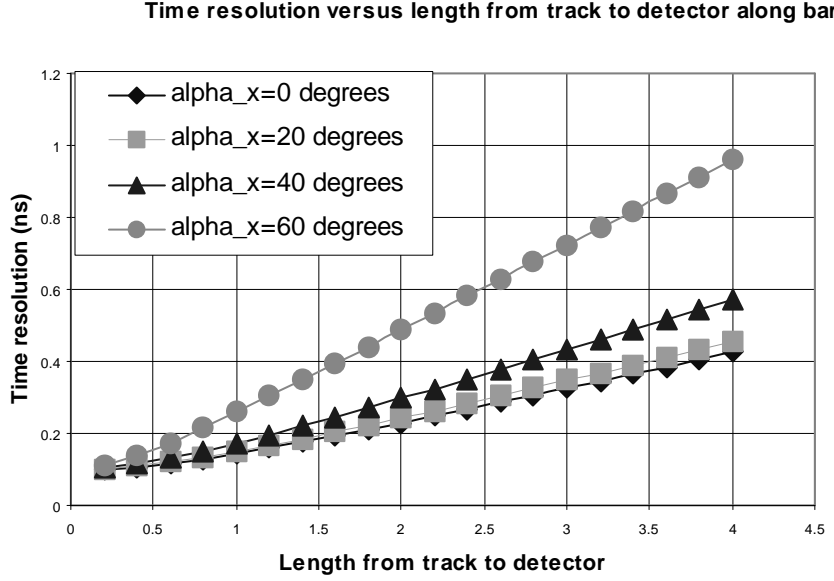


Figure 6. Observed time resolution versus length along the bar from track to detector expected for the particular case described in the text. The track enters the bar normally in both projections.

4.4 Detectors

The availability of detectors continues to be “the” crucial element for design. Conventional PMTs remain hard to beat for the price-to-performance ratio. In the last few years, metal channel PMTs have become available that may allow a more elegant “lens-focused” design. These may be becoming competitive in cost and performance, although it is not quite obvious if an adequate packing fraction can be obtained for the imaging requirements of a 3-D device. The newest flat panel PMTs by Hamamatsu [21] may provide a solution to this problem. Hybrid PMTs could also be a promising alternative for the future [19]. Other potential technologies, such as Avalanche Photodiodes [16], visible light gas detectors, VLPCs, and MCP-PMTs are more speculative. Although it is clearly difficult to imagine using a Transition Edge Sensor (TES) [20] since it requires 40 mK temperatures, it is an exciting new high-efficiency device that has the amazing feature that it can measure the energy resolution of a visible photon to about 0.15 eV. This could

reduce the chromatic term in the resolution equation by over a factor of ten (see Sec. 5.1.2 below). On the other hand, it is a slow detector, and would not allow one to take full advantage of the timing properties of DIRCs. Another way to reduce the production chromatic smearing term is described below in Sec. 5.1.2.

4.5 Combinations of Design Elements

The design elements discussed above can be “mixed and matched,” but only some combinations make sense. In general, to obtain the best performance and background rejection in most modern experimental environments, it seems best to use detectors that have relatively high precision in both space and time.

As an exercise, consider the design elements of the BaBar DIRC:

1. Light production: fused silica.
2. Light transport: two-dimensional (pipe).
3. Imaging principle: two-dimensional pinhole.
4. Detector: two-dimensional in space, conventional PMT, timing used primarily to resolve ambiguities and backgrounds; nonmodular matching between detectors and bars reduces pixel count.
5. Expected performance: 4σ π - K separation to ~ 4 GeV/c (depending on track dip angle).

Another version of this counter might use similar bar-boxes to those in the BaBar DIRC but they might contain only one “plate” style DIRC bar (about 40 cm in width) with a pixilated array detector like the following:

1. Light production: fused silica.
2. Light transport: one-dimensional (plate style).
3. Imaging principle: fully 3-D; proximity focused in wide plate dimension; reflective lens focused in the narrow dimension; fast timing used to measure the chromatic term, resolve ambiguities (including the side bounce ambiguities), and resolve backgrounds (see section 5 below).

4. Detector: closely packed, fast two-dimensional pixilated Flat Panel PMTs (64 6x6mm pixels per PMT) with good timing (~ 100 ps; non-modular matching between detectors and bars reduces pixel count).
5. Expected performance: 4σ π - K separation to ~ 5 GeV/c (depending on track dip angle).

In contrast, suppose one wished to design an inexpensive DIRC for a medium energy fixed-target experiment. One might consider design elements such as the following:

1. Light production: acrylic.
2. Light transport: one-dimensional (plate) downstream of the target.
3. Imaging principle: proximity focused in the wide plate dimension; reflective focused through a molded plastic lens in the narrow pin-hole dimension; timing used mostly to resolve ambiguities and reject backgrounds.
4. Detector: metal channel PMT with 1×64 pixels (1 cm \times 1 mm pixels).
5. Expected performance: 4σ π - K separation to ~ 4 GeV/c, but with limited angular coverage.

5. Resolution Issues

In a simple model, the resolution on the Cherenkov angle for a given track $\sigma[\theta_c(\text{tot})]$ is given by

$$\sigma[\theta_c(\text{tot})] = \frac{\sigma[\theta_c]}{\sqrt{N_{pe}}}, \quad (10)$$

where N_{pe} is the total number of photons detected, and the angular resolution on the projected track ($\sigma[\alpha_{\text{Track}}]$) is assumed to be sufficient [$\sigma[\alpha_{\text{Track}}] \ll \sigma[\theta_c(\text{tot})]$] so it does not contribute to the overall resolution. The error on each individual photon $\sigma[\theta_c]$ is given in terms of the design components discussed in Section 4 as [1,2];

$$\sigma[\theta_c] = \sqrt{\sigma[\theta_{\text{Production}}]^2 + \sigma[\theta_{\text{Transport}}]^2 + \sigma[\theta_{\text{Imaging}}]^2 + \sigma[\theta_{\text{Detection}}]^2}, \quad (11)$$

The dominant smearing term at production ($\sigma[\theta_{\text{Production}}]$) is the so-called production chromatic term ($\sigma[\theta_{\text{Chromatic}}]$). This term arises from the fact that the refractive index $n(\lambda)$ is a function of photon wavelength, as described by Eq. (1). The value of ($\sigma[\theta_{\text{Chromatic}}]$) is about 5.4 mrad for the BABAR DIRC detector or any other detector with similar photon wavelength bandwidth. Other production smearing terms, such as trajectory distortion due to bending in the magnetic field, or multiple scattering in the radiator material are much smaller, at least at high momentum where good resolution is required to separate π s from K s.

Transport smearing ($\sigma[\theta_{\text{Transport}}]$) may be caused by various flaws in the DIRC radiators, such as non-parallel sides, non-planar surfaces, and non-orthogonal sides and faces. Due to effects of these kinds, the resolution contribution from this term tends to grow as the square root of the propagation length. In BaBar DIRC, the most difficult effect of this kind to control was the side-to-face orthogonality, which contributes around 2-4 mrad per photon for a bar at the production specification limit. In principle, such effects can be made much smaller with different production methodology (at a higher cost), or by using a one-dimensional transport design to limit the number of side bounces.

It is convenient to consider the last two terms ($\sigma[\theta_{\text{Imaging}}]$, $\sigma[\theta_{\text{Detection}}]$) together. The basic principles have already been described in section 4.3. In principle, angular resolution derived from positional information can be made “arbitrarily” good to match requirements for a particular performance limit. In particular, the imaging component that comes from the bar size in a pin hole focusing scheme, such as the one used by BaBar, can be made small with lens focusing, and the number of detector pixels and the standoff distance are essentially arbitrary choices. It makes economic sense to choose focusing methods and detector configurations that balance the various resolution components.

Excellent single photoelectron time resolution is required to contribute in a meaningful way to equivalent single photon angular resolution. For example, for a BaBar-style DIRC, one needs a time resolution of about 200 ps per photon to be somewhat (i.e., within about a factor of two)

competitive with the positional photon information for a track at a zero degree track dip angle (see Figure 5). At larger track dip angles, the performance will be less competitive. Because of the chromatic dispersion in the travel time, it is not feasible (at least with the detection bandwidth of a bi-alkali PMT) to obtain a much better resolution from the time dimension, unless the photon wavelength can be measured (see below).

5.1 DIRC Performance Limits

For a $\beta \approx 1$ particle of momentum (p) entering a radiator with index of refraction (n), the number of σ separation (N_σ) between particles of mass (m_1) and (m_2) is approximately

$$N_\sigma \approx \frac{\left(m_1^2 - m_2^2 \right)}{\left(2p^2 \sigma[\theta_c(\text{tot})] \sqrt{n^2 - 1} \right)}. \quad (12)$$

The large index of refraction in the DIRC radiator makes the term $\sqrt{n^2 - 1}$ rather large (at least compared to gas radiators). Thus, the DIRC will have good performance only in the low and medium momentum regions. In particular, obtaining good resolution much above 4 GeV requires excellent angular resolution. For example, 4σ separation between pions and kaons requires a resolution on $\sigma[\theta_c(\text{tot})]$ of about 1.5 mrad at 4 GeV/c, and about 0.25 mrad at 10 GeV/c.

The fundamental limits on the DIRC technique are primarily (1) N_{pe} ; (2) chromatic smearing; and (3) practically, but less fundamentally, systematic limits on bar production quality and alignment. In the following, we briefly review how one might mitigate each of the first two components.

5.1.1 Photon Statistics

In principle, one could increase the bar thickness to increase the photoelectron number, although this would increase the material in the particle's path. Solid-state detectors could also attain two to

three times the photon detection efficiency of typical PMTs, and thus increase the number of photoelectrons observed substantially. However, in itself, an increase in statistics leads to a rather modest improvement in performance since the resolution only improves as the square root of the number of photons, in the best case. As an example, consider a very optimistic case where the transverse angles are sufficiently well measured that the individual photon resolution is dominated by the 5.4 mrad per photon production chromatic smearing of a fused silica radiator, working with a bi-alkali photocathode with a borosilicate window, and where the radiator is sufficiently thick to give 100 photoelectrons. Even so, the 4σ separation limit between π s and K s is just above 6 GeV/c.

5.1.2 Mitigating Chromatic Smearing

It seems impractical to apply chromatic correction in the focusing system, or to find a radiator with significantly less dispersion than fused silica. However, the high efficiency of a solid-state detector could allow one to reduce the energy range of accepted Cherenkov photons. Somewhat counter-intuitively, this can actually improve the total resolution substantially in a DIRC designed so that the chromatic term dominates, even though such a restriction limits N_{pe} substantially. For example, the total contribution $\sigma[\theta_c(\text{tot})]$ from the chromatic term is reduced by a factor of 2.5 when the photon energy range is restricted between 600 and 450 nm compared to the case where all photons between 600 nm and 300 nm are accepted, even though the number of photons observed is reduced by nearly a factor of four!

The “ideal” solution to the chromatic smearing would be a detector that measures the photon energy directly. In principle, the TES device described above could do this, but is slow and would be very hard to implement. It seems more practical to use the large dispersion of n_g , as described earlier, to measure the photon wavelength directly in a 3-D DIRC [22]. That is, by comparing the individual photon flight time with its measured angle, the photon wavelength can be calculated. This allows the refractive index at production to be rather precisely calculated so that the chromatic piece of the production term can be substantially reduced. Figure 7 shows that the measurement of photon wavelength done this way can be quite accurate if the time resolution is good (100ps). Looked at in the Cherenkov angle space, this is equivalent to reducing the smearing due to chromaticity to less

than 0.2 mrad for a photon travel length of 6 m. The large chromatic dispersion of the group velocity actually works in one's favor in this case!

In fact, even with a time resolution like that of BaBar (~ 1.6 ns), one can measure the ~ 5.4 mrad chromatic production term to ~ 200 %/L(meters) (i.e., for typical lengths of 3-6 meters, ~ 3.6 - 1.8 mrad). Of course, this reduction in the chromatic term is not very helpful in the present BaBar DIRC, as the precision of the angular measurement is dominated by the imaging piece.

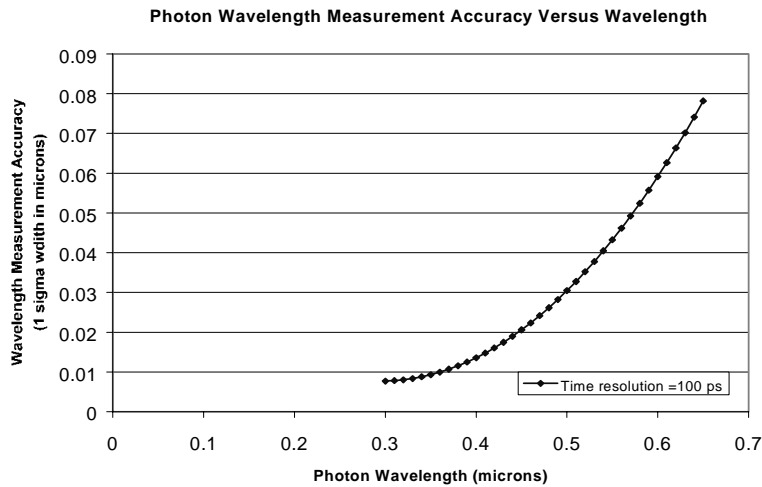


Figure 7. Resolution on the wavelength measurement versus wavelength per detected photon for an assumed time resolution of 100 ps at a propagation length of 6 meters. This calculation assumes that the transverse propagation angles (α_x, α_y) are sufficiently well measured that the time resolution is the only important term.

6. Summary

DIRCs are robust, fast particle identification devices, well-suited to high-radiation environments. The first generation BaBar DIRC has been operating with colliding beams since May 1999, with performance that is quite near that predicted from Monte Carlo simulation. The design of elegant second generation DIRCs either for new experiments or possible upgrades to BaBar depends greatly on the availability of appropriate photon detectors. Though such detectors would allow more

flexible designs, the momentum range of application for DIRCs is inherently limited. The “natural” momentum separation range for good π /K separation in a DIRC is up to about 4-5 GeV/c. It is plausible, but quite difficult, to increase this range by another factor of about two.

ACKNOWLEDGMENTS

I would like to thank all of the members of the DIRC BaBar collaboration, whose work to build and then analyze data from this new device has been instrumental to increasing my understanding of essential features of this type of detector. I would like to give special thanks for discussions on specific items addressed in this paper to Dave Aston, Richard Blankenbecler, Mark Convery, Gautier Hamel de Monchenault, Andreas Hoecker, David Leith, Brian Meadows, Al Odian, Moishe Pripstein, Jochen Schwiening, Stephan Spanier, Jaroslav Va’Vra, Christophe Yelle, and Marco Zito.

BIBLIOGRAPHY

1. B. Ratcliff, BaBar NOTE 92; “The B Factory Detector for PEP-II: A Status Report”, published in Proceedings of the International Conference on High Energy Physics, 1889-1896 (1992); and SLAC-PUB-6047 (1993), published in Tsukuba B Factories, 331-341 (1992).
2. P. Coyle *et al.*, Nucl. Instrum. and Methods A **343**, 292 (1994).
3. D. Aston *et al.*, IEEE Trans. Nucl. Sci. **42**, 534-538 (1995) and SLAC-PUB-6731 (1994).
4. C. Lu *et al.*, Nucl. Instrum. and Methods A **371**, 82-86 (1996).
5. T. Kamae *et al.*, Nucl. Instrum. and Methods A **382**, 430-440 (1996).
6. H. Staengle *et al.*, Nucl. Instrum. and Methods A **397**, 261-282 (1997).
7. Kichimi *et al.*, Nucl. Instrum. and Methods A **371**, 306-310 (1994).

8. M. Akatsu *et al.*, DPNU-99-08 (1999), and T. Ohshima, Nucl. Instrum. and Methods A **453**. 331-335 (2000).
9. See, for example, J. Schwiening *et al.*, SLAC-PUB-8590 (2000), invited talk presented at 30th International Conference on High-Energy Physics (ICHEP 2000) Osaka, Japan, and I. Adam *et al.*, Nucl. Instrum. and Methods A **453**. 301-307 (2000).
10. See, for example, G. Lynch, B. Ratcliff and J. Veillet, private communication.
11. B.N. Ratcliff and S. Spanier, Nucl. Instrum. and Methods A **433**, 456-463 (1999).
12. I. Tamm, J. Phys. U.S.S.R. 1,439 (1939).
13. H. Motz and L. I. Schiff, Am. J. Phys., **21** 258-259 (1953).
14. See, for example, J. D. Jackson, “Classical Electrodynamics”, 4th Ed., 211(1965).
15. G. Kettenring, Nucl. Instrum. and Methods **131**, 451-456 (1975).
16. R. Wilson, Nucl. Instrum. and Methods A **433**, 487-491(1999).
17. K. Honscheid, M. Selen, and M. Sivertz, Nucl. Instrum. and Methods A **343**. 306-310 (1994).
18. I. Adam *et al.*, SLAC-PUB I -7707, Nov. 1997, and IEEE Trans.Nucl.Sci.45: 450-455 (1998).
19. A. Braem *et al.*, Nucl. Instrum. and Methods A **433**, 153-158 (1999).
20. B. Cabrera *et al.*, Applied Physics Letters **73**, 735-737 (1998).
21. Hamamatsu Photonics K.K., <http://www.hamamatsu.com/>.
22. This approach has been broadly discussed within the BaBar DIRC group, and has been particularly emphasized by Brian Meadows.